Threshold fluence and incubation during multi-pulse ultrafast laser ablation of quartz

RAFFAELE DE PALO,[1,*] ANNALISA VOLPE,[1,2] CATERINA GAUDIUSO,[1,2] PIETRO PATIMISCO,[3,4] VINCENZO SPAGNOLO,[3,4] AND ANTONIO ANCONA[1,2]

[1]*Dipartimento Interateneo di Fisica, Università degli Studi di Bari, Bari, Italy*
[2]*CNR-IFN UOS BARI, Via Amendola 173, Bari, Italy*
[3]*PolySense Lab, Dipartimento Interateneo di Fisica M. Merlin, Università degli Studi di Bari Aldo Moro e Politecnico di Bari, Via G. Amendola 173, Bari 70125, Italy*
[4]*PolySense Innovations srl, Via Amendola 173, Bari 70126, Italy*
*raffaele.depalo@uniba.it

Abstract: In this work, the incubation effect on the laser ablation threshold of quartz, after multi-shot irradiation with femtosecond pulses at 1030-nm-wavelength with different repetition rates, was investigated. A strong decrease of the multi-pulse ablation threshold with the number of pulses N was found due to incubation. Moreover, the influence of the repetition rate was negligible in the investigated frequency range which went from 0.06 to 200 kHz. A saturation of the threshold fluence value was observed at number of pulses $N > 100$ which has been found to be well fitted by an exponential incubation model. Using such model, we estimated the single-pulse ablation threshold value and the incubation coefficient for quartz, which were found equal to $F_{th,1} = 6.23 \pm 0.23$ J/cm^2 and $k = 0.058 \pm 0.004$.

1. Introduction

Quartz is the crystalline form of silicon dioxide, and it is one of the most abundant minerals found on earth. It is a hard (7 on Mohs scale), chemically stable and piezoelectric [1] material with a high melting point (>1600 °C). From the electrical and optical point of view, quartz is a transparent dielectric from the UV to the near IR region. Aside from traditional industrial fields, such as glass making, jewellery and watchmaking, in the last two decades, quartz has been also employed for sensing technology applications, for example as Quartz-Crystal-Microbalance (QCM) [2] or Quartz-Tuning-Forks (QTFs) [3]. QCMs are predominantly used as electrochemical sensors [4], while QTFs are mainly used in Quartz-Enhanced-Photoacoustic-Spectroscopy (QEPAS) [5] or Light-Induced-Thermoelastic-Spectroscopy (LITES) [6,7]. Micromachining of quartz can be realized through various techniques such as diamond cutting, lithography, wet and dry etching, and ion beam etching. These techniques are well established and widely used but have some drawbacks, like chemical contamination, limited processing resolution and long processing times. A convenient and reliable alternative is represented by Ultra-Short-Pulsed-Laser (USPL) processing. This method neither requires preliminary chemical treatment of samples nor expensive lithographic masking. The laser machining speed is much faster than other mechanical methods and tight focusing of the laser beam can lead to highly localized treatment of materials with micrometric spatial resolution [8]. USPL has been applied efficiently to quartz for drilling [8] and stealth dicing [9]. One of the emerging area of USPL processing is represented by the micro- and nano-texturing aiming to change the mechanical [10], electrical [11] and optical [12] properties of materials. Micro- and nano-texturing of any material requires preliminary knowledge of the ablation threshold, defined as the minimum laser fluence to start the material removal. For a great number of materials, from the most common metals such as tungsten, iron, nickel [13] and steel [14] to synthetic ceramics [15], the ablation threshold is lowered when the

surface is irradiated with multiple consecutive fs-pulses. This effect is referred to as incubation and was firstly observed for ablation of metals using nanosecond laser pulses [16] and then it has been implemented also for semiconductors [17] and dielectrics [18] in the femtosecond pulses regime. As a result of incubation, the material optical absorption increases at each pulse, so that for the subsequent pulse the excitation of free carriers is enhanced, and the ablation threshold value is reduced. The physical mechanisms causing incubation are still not clear, especially for metals. The most proposed hypothesis on the origin of incubation in metals is related to an increase in surface roughness leading to the enhancement in the material optical absorption [19].

The dependence of multi-pulse ablation threshold $F_{th}(N)$ from the number of pulses N and from the single-pulse threshold $F_{th,1}$, was originally described through a power law, introducing an incubation coefficient S [16]. This model was modified by Di Niso et al. [20] with the introduction of a constant fluence threshold $F_{th,\infty}$ which represents an asymptotic threshold value when N tends to infinity. This model has been used most often for metals such as steel [21], copper, iron [19] and zirconia alumina [22].The asymptotic threshold value $F_{th,\infty}$ has been introduced also in a further incubation model proposed for dielectric materials by Rosenfeld et al. [18]. This model has been used for dielectrics such as fused silica, sapphire, CaF_2 [18,23,24] but also semiconductors as GaN [25].

The multi-pulse ablation threshold and incubation have been extensively studied for various dielectric materials, like sapphire [24,26] and fused silica [27], but not so far for quartz.

In this paper we systematically estimated the multi-pulse ablation threshold of quartz with 200 femtosecond-pulses at different number of pulses N, ranging from 5 to 10000. The incubation mechanism was investigated trying to assess which of the incubation models present in literature was best suited to describe this phenomenon in case of quartz. Finally, the influence of repetition rate, in the range from 0.06 kHz up to 200 kHz, on both the multi-pulse ablation threshold and the incubation coefficient was studied.

2. Materials, experimental setup, and methods

2.1. Materials

The quartz samples, consisting of double polished z-cut quartz wafers with an area of 24.5×24.5 mm^2 and a thickness of 400 µm. The samples were purchased from Nano Quartz Wafer GmbH.

2.2. Experimental setup

The set-up employed for the experiments is schematically shown in Fig. 1.

A Pharos SP 1.5 laser system from Light Conversion was employed. It emits an almost diffraction limited beam ($M^2 = 1.3$, certified by the laser producer) with 200 fs pulses, characterized by a central wavelength at 1030 nm, a maximum average power of 6 W and a maximum pulse energy E_P of 1.5 mJ. The repetition rate f was tunable from single pulse to 1 MHz. The linearly polarized laser beam passed through a half-wave plate and a polarizer to ensure a fine tuning of the laser power. The linear polarizer transmitted the P component of polarization. The laser beam was then sent to a PC-controlled galvo scanner mounting a 100 mm-F-theta lens. The estimated beam waist w in air was 16 µm. The quartz samples were placed on the focal plane of the F-theta lens. Four series of ablation craters were produced, arranged along squared matrices, each series at a different value of repetition rate f. Every series consisted of several matrixes; each matrix was produced at N (from $N = 5$ to $N = 10000$) and within each matrix, each row of craters was ablated with a fixed E_P value. The ablated craters diameters D were measured using an optical microscope (Nikon Eclipse E600). Images of each crater were acquired, and their diameter D was directly measured using the microscope acquisition software. In Fig. 2 the image of a representative matrix realized at $f = 6$ kHz and $N = 100$ is shown.
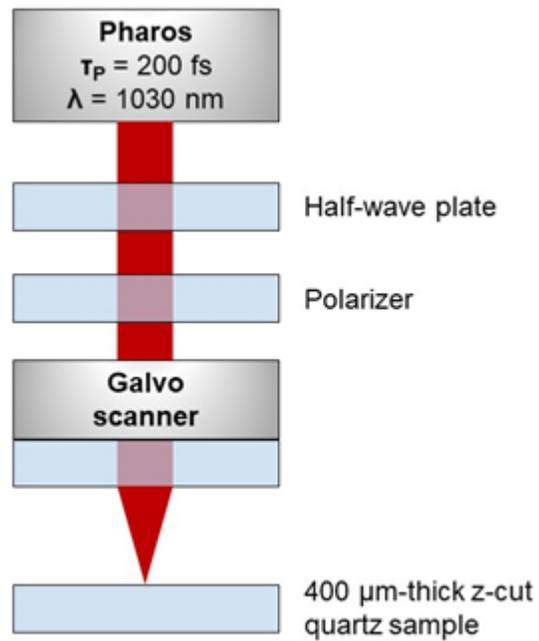
Fig. 1. Sketch of the experimental setup.
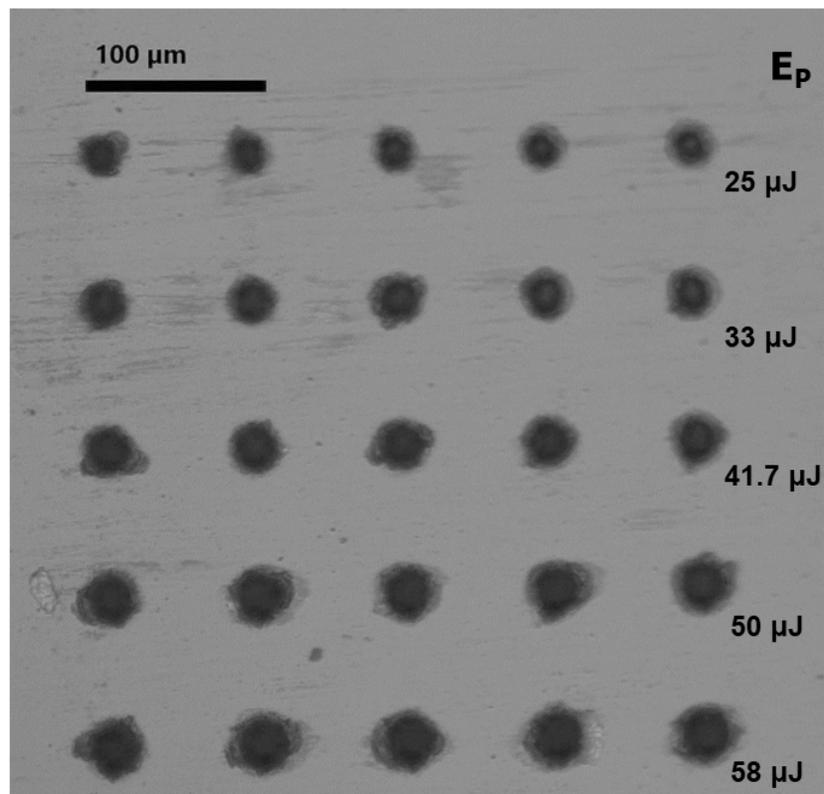
Fig. 2. Dot matrix realized at $f = 6$ kHz and $N = 100$ pulses. The pulse energies for craters within each row from top to bottom are: 25 µJ, 33 µJ, 41.7 µJ, 50 µJ and 58.3 µJ

In Table 1 the working laser parameters (pulse energies, repetition rates and number of pulses) are summarized.

Table 1. Laser working parameters

	$f = 0.06, 6, 60$ [kHz]	$f = 200$ [kHz]
Pulse Energy E_P [µJ]	25 - 33.3 - 41.7 - 50 - 58.3	17.2 - 20 - 23.2 - 25.3
Number of Pulses N	5-10-20-50-100-500-1000-2000-5000-10000	10-20-50-100-500-1000-2000-5000-10000

2.3. Methods

The multi-pulse threshold fluence $F_{th}(N)$ was estimated for each N value (namely for each matrix), using the procedure introduced by Liu et al. [28]. This approach assumes a Gaussian spatial energy distribution for the laser beam. The threshold fluence for N consecutive laser pulses $F_{th}(N)$ is related to the crater squared diameter D^2 through the following equation:

$$D^2 = 2w^2 \ln\left(\frac{F_0}{F_{th}(N)}\right) \tag{1}$$

where the peak laser fluence F_0 is defined as:

$$F_0 = \frac{2E_P}{\pi w^2} \tag{2}$$

and w is the laser beam FWHM. Using the previous two equations, the squared diameters D^2 can be linearly fitted as a function of the logarithm of the pulse energies E_P in order to determine the
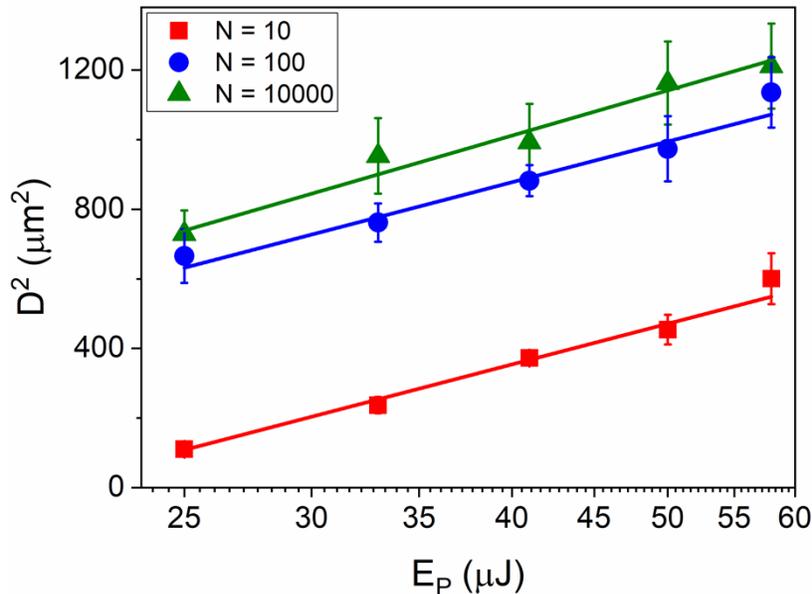
Fig. 3. D^2 vs E_P semi-logarithmic plots at $f = 0.06$ kHz for $N = 10$ (red squares), $N = 100$ (blue squares) and $N = 10000$ (green squares) with the relative linear fits. Each experimental point is the average value of the crater squared diameters D^2 realized at the same pulse energy E_P. Figure 3 clearly shows that the diameter grows either by increasing the pulse energy or the number of pulses.

laser FWHM w and the multi-pulse threshold fluence $F_{th}(N)$. This procedure was repeated for each selected value of N and repetition rate to estimate $F_{th}(N)$ and the beam waist w, found equal to 16 ± 0.08 μm. In Fig. 3, three representative semi-logarithmic plots at $f = 0.06$ kHz are shown together with the relative linear fits.

3. Results

In Fig. 4 the multi-pulse thresholds fluence at $f = 0.06$ kHz are shown as a function of N.
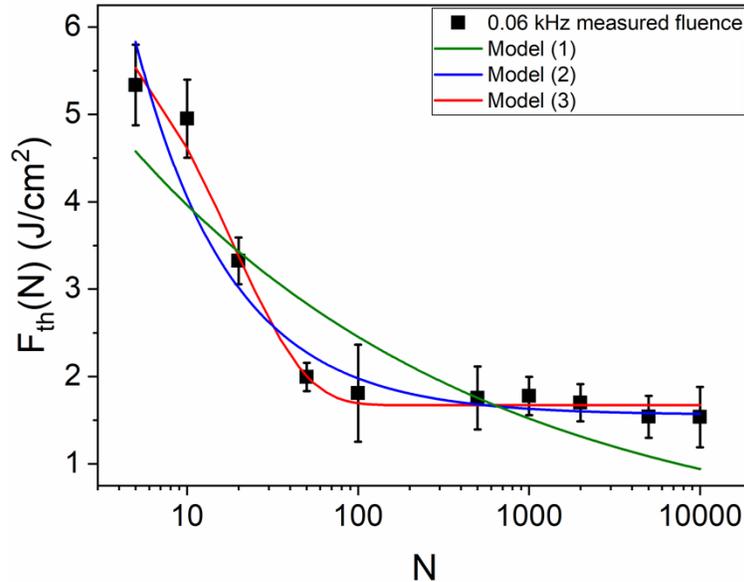
Fig. 4. Multi-pulse threshold fluence (black squares) $F_{th}(N)$ as a function of the number of laser pulses N, at $f = 0.06$ kHz. The experimental data are fitted with three different models (green, blue, and red curves).

The experimental data (black squares) show that $F_{th}(N)$ decreases rapidly for $N < 100$. Then reach a plateau. This $F_{th}(N)$ trend can be ascribed to the incubation effect.

Three different models were used to fit the experimental data in Fig. 4. Model (1) (green curve in Fig. 4) was proposed for the first time by Jee et al. [16] and predicts that:

$$F_{th}(N) = F_{th,1} N^{S-1} \tag{3}$$

This model relates the multi-pulse threshold fluence $F_{th}(N)$ to the single pulse threshold fluence $F_{th,1}$ by means of a power law which introduces the incubation coefficient S, which is an empirical parameter that depends on the strength of the incubation in the target material and is bound between 0 and 1 ($0 < S < 1$). If $S = 1$, incubation is absent, and the ablation threshold is not dependent from N. For $S < 1$ incubation takes place, and the closer S is to zero, the faster the ablation threshold decreases. Model (2) (blue curve in Fig. 4) was introduced by Di Niso et al. [21] to take into account the experimental observation that, differently from what predicted by Model (1), the threshold fluence saturated to an asymptotic value different from zero in case of irradiation with a relatively high number of pulses (typically $N > 100$). For this reason, an offset value $F_{th,\infty}$, representing the saturating threshold fluence for very large number of pulses N, was

introduced and the following expression for the incubation model was proposed:

$$F_{th}(N) = F_{th,\infty} + [F_{th,1} - F_{th,\infty}]N^{S-1} \tag{4}$$

Model (3) (red curve in Fig. 4) follows the exponential law proposed by Rosenfeld et al. [29]:

$$F_{th}(N) = F_{th,\infty} + [F_{th,1} - F_{th,\infty}]e^{-k(N-1)} \tag{5}$$

Similarly, to the model of Di Niso et al., also here a saturation of incubation is considered for very high numbers of N through the offset $F_{th,\infty}$. The factor k represents the incubation coefficient, which is, as the coefficient S, of empiric nature and depends on the strength of incubation in the target material. Differently from S that can assume only values comprised in the range between 0 and 1, k can assume any value depending on the strength of the incubation effect in the material.

Table 2 summarizes the results of the fits shown in Fig. 4, of the experimental data with the three different incubation models proposed in literature. The fitted parameters are $F_{th,\infty}$ for Model (2) and (3), $F_{th,1}$ for all three models, S for Model (1) and Model (2), k for Model (3). Finally, the value of R^2 coefficient is also reported to compare how well the different models fit the experimental data.

Table 2. Results of the experimental fits in Fig. 4

	Model (1)	Model (2)	Model (3)
$F_{th,\,\infty}$ [J/cm^2]	-	1.56 ± 0.16	1.67 ± 0.05
$F_{\mathbf{th,1}}$ [J/cm^2]	6.40 ± 1.29	14.87 ± 4.54	6.47 ± 0.33
S[-]	0.79 ± 0.05	0.22 ± 0.15	-
k[-]	-	-	0.054 ± 0.004
R^2	0.626	0.918	0.987

A comparison among R-squared values showed that Model (3) provides the best fit to the experimental data. Thus, Model (3) has been chosen to fit the data also at others repetition rates. A more detailed discussion will be provided in the next section.

In Fig. 5 the experimental multi-pulse fluence $F_{th}(N)$ trends are shown as function of N at all the investigated repetition rates f, fitted with the exponential law given by Model (3).

The parameters extracted from the experimental fits are reported in Table 3.

Table 3. Results of the Model 3 fits performed at the four different repetition rates (Fig. 5)

f [kHz]	$F_{th,\,\infty}$ [J/cm^2]	$F_{th,1}$ [J/cm^2]	k [-]
0.06	1.67 ± 0.05	6.47 ± 0.05	0.054 ± 0.004
6	1.68 ± 0.06	6.02 ± 0.30	0.051 ± 0.009
60	1.73 ± 0.05	6.42 ± 0.32	0.058 ± 0.007
200	1.71 ± 0.08	6.23 ± 1.13	0.063 ± 0.013
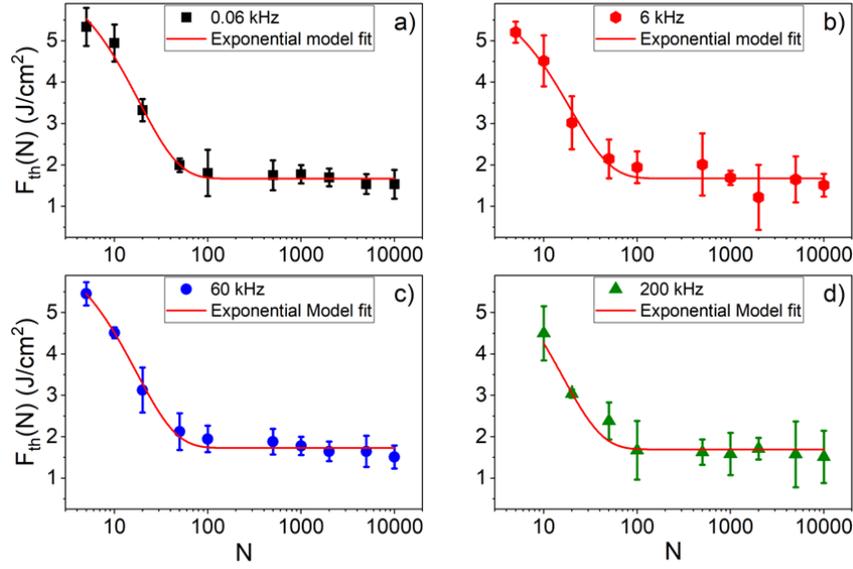
Fig. 5. Model 3 fits of $F_{th}(N)$ versus the number of laser pulses N: (a) $f = 0.06$ kHz (black squares), (b) $f = 6$ kHz (red hexagons), (c) $f = 60$ kHz (blue dots), (d) $f = 200$ kHz (green triangles).

4. Discussion

4.1. Incubation models

In dielectric and semiconductor materials the incubation effect is caused by the accumulation of laser induced defects sites [18]. When a laser pulse has a fluence below the single-pulse threshold, the free carriers excited by the pulse will relax, generating defects sites, as color centers or Frenkel pairs [18]. Sites can generate additional energy levels within the band-gap region of the material. These new levels represent additional excitation routes for the carriers from the valence band, promoting additional absorption channels for subsequent laser pulses at fluence below the single-shot threshold. The defect density will increase pulse-by-pulse until it reaches saturation [30]. Correspondingly, the multi-pulse fluence threshold will decrease with N until it reaches the saturation value $F_{th,\infty}$. This process is often referred to as metallization, because it causes the filling of the dielectric band gap with energy states, resulting in a metal-like electronic band structure. Similarly, in quartz the accumulation of band-gap defects during irradiation with multiple pulses might explain the incubation effect. In their work on fused silica, Duan et al. [31] proposed that the number of color centers increases exponentially with the number of pulses N as described by the following equation:

$$D(I) = \frac{k_p}{k_p + k_c} D_p(0)[1 - e^{-(k_p+k_c)I}] \quad (6)$$

where $D_P(0)$ is the intrinsic defect density of the material, k_p and k_c are conversion rates of intrinsic defects into color centers and I is the total laser pulse radiation flux, which is directly proportional to N. The one minus negative exponential of I factor clearly indicates that the defect density saturates with the number of pulses N. This saturation effect is the same observed in the reduction of multi-pulse ablation threshold with the number of pulses N. However, the question remains which one of the models found in literature and presented in section 3, is the best suited to describe the incubation effect observed on quartz. The results in Table 2 indicate that Model

(1) predicts $F_{th,1} = 6.40 \pm 1.29$ J/cm^2 and $S = 0.79 \pm 0.05$ in good agreement with values found for other dielectrics [32,33,26], but fails to take into account the saturation effect for $N > 100$ as demonstrated by the low R^2 value of 0.626. Model (2) correctly predicts the saturation effect, returning $F_{th,\infty} = 1.56 \pm 0.16$ J/cm^2 and, indeed, the fitting of the experimental data returns an of $R^2 = 0.918$, higher than Model (1). However, Model (2) largely overestimates the fluence threshold with single pulse $F_{th,1} = 14.87 \pm 4.54$ J/cm^2, as well as it underestimates the incubation coefficient $S = 0.22 \pm 0.15$. Additionally, the values of both parameters are quite different from the values that can be found in literature on other dielectric materials [24]. Fitting data with Model (3) results in the largest R^2 value of 0.987, which means that this model predicts more properly the incubation effect on quartz, returning a fluence threshold saturation value $F_{th,\infty} = 1.67 \pm 0.05$, a single-shot threshold $F_{th,1} = 6.47 \pm 0.33$ and an incubation coefficient $k = 0.054 \pm 0.004$. The value found for $F_{th,1}$ is comparable to those already found for quartz in other works [34,35]. No studies on the incubation effect in quart have been found in literature, but the k value estimated in this work is comparable to those found for other transparent dielectrics, such as sapphire [24]. This result suggests that Model (3) is the best one suitable to describe the experimental data in Fig. 4 and the incubation effect in transparent dielectric; this conclusion cannot be extended to opaque dielectrics since no works were found investigating incubation in such materials

4.2. Influence of repetition rate

The results in Table 3 clearly show that there is no influence of the repetition rate on the multi-pulse ablation threshold in the frequency range investigated in this work. $F_{th,1}$ does not depend on frequency, so an average value can be calculated, and it results $F_{th,1\ av} = 6.23 \pm 0.23$ J/cm^2. This value is comparable with the $F_{th,1}$ (5 J/cm^2) found for quartz ablation by Xu et al. [35]. Same discussion can be argued for $F_{th,\infty}$ and k, within the corresponding uncertainty intervals; therefore, also these two quantities do not depend on the repetition rate. This result can be explained by considering the lifetime τ of the defects induced by the laser irradiation, which has been estimated to be around 50 ms by Costache et al. [30]. In their work the authors analyzed ion desorption kinectis and defect dynamics from BaF$_2$ and CaF$_2$ crystal after femtosecond laser excitation. They used a Ti:Sapphire CPA laser system emitting 120 fs pulses of 800 nm. They measured the laser-induced defect relaxation time in CaF$_2$ and BaF$_2$ crystals through flourescence detection using a ICCD camera. Laser induced fluorescence was detected at laser intensities near the single pulse damge threshold for the two crystals, ~30TW/cm^2 for CaF$_2$ and ~20TW/cm^2 for BaF$_2$. The longest pulse-to-pulse temporal separation experienced in this work is 17 ms, corresponding to a repetition rate of $f = 0.06$ kHz. For higher frequencies, this time delay is even shorter. Therefore, at the repetition rates investigated in this work, the defects quickly accumulate this can explain why no influence of the repetition rate was observed in the measurements. The average values for $F_{th,\infty}$ and k can be also calculated and found to be $F_{th,\ \infty} = 1.70 \pm 0.06$ J/cm^2 and $k = 0.058 \pm 0.006$. No reference in literature were found on these quantities for quartz, but they are comparable with those measured for sapphire [24,36].

5. Conclusion

We performed a systematic investigation of multi-pulse ablation threshold fluence $F_{th}(N)$ on quartz using different number of pulses N, from 5 up to 10000. An incubation effect with a decrease of $F_{th}(N)$ with N was observed. For $N > 100$, $F_{th}(N)$ rapidly saturated reaching an asymptotic value indicated as $F_{th,\infty}$. The exponential model previously reported by Rosenfeld et al. [18] was found to be the best suited to describe such incubation effect for quartz. The measured value for the single pulse ablation threshold $F_{th,1}$ agrees with those already found for quartz, and the estimated values of $F_{th,\infty}$ and the incubation coefficient k are comparable with those found for other transparent dielectric materials, such as sapphire, in similar irradiation conditions. The accumulation of laser-induced defects during multi-pulse irradiation was recognized as

responsible for the observed incubation effect. This would also explain why no dependence of the ablation threshold and incubation coefficient on the repetition rate was found in the investigated range, for *f* from 0.06 kHz to 200 kHz. In this frequency range, the laser-induced defects lifetime is expected to be much longer than the inter-pulse delay, thus defects accumulate exponentially in all the investigated conditions. This study provides the operating conditions and parameters useful for laser processing of quartz with ultrashort pulses at high repetition rates for applications such as the enhancement of quartz optical absorption in near- and mid-infrared range and the investigation about Laser-Induced-Periodic-Surface-Structures (LIPSS) on quartz surface

Disclosures. The authors declare no conflicts of interest.

Data availability. Data underlying the results presented in this paper are not publicly available at this time but may be obtained from the authors upon reasonable request.

References

1. Y. Saigusa, "Quartz-Based Piezoelectric Materials," Adv. Piezoelectric Mater. **2**, 197–233 (2017).
2. R. E. Speight and M. A. Cooper, "A Survey of the 2010 Quartz Crystal Microbalance Literature," J. Mol. Recognit. **25**(9), 451–473 (2012).
3. P. Patimisco, A. Sampaolo, H. Zheng, L. Dong, F. K. Tittel, and V. Spagnolo, "Quartz-enhanced photoacoustic spectrophones exploiting custom tuning forks: a review," Adv. Phys.: X **2**(1), 169–187 (2017).
4. D. A. Buttry, "Applications of the Quartz Crystal Microbalance to Electrochemistry," J. Phys. Chem. **91**(6), 1292–1295 (1987).
5. A. Sampaolo, P. Patimisco, M. Giglio, A. Zifarelli, H. Wu, L. Dong, and V. Spagnolo, "Quartz-enhanced photoacoustic spectroscopy for multi-gas detection: A review," Anal. Chim. Acta **1202**, 338894 (2022).
6. S. Dello Russo, A. Zifarelli, P. Patimisco, A. Sampaolo, T. Wei, H. Wu, L. Dong, and V. Spagnolo, "Light-induced thermo-elastic effect in quartz tuning forks exploited as a photodetector in gas absorption spectroscopy," Opt. Express **28**(13), 19074 (2020).
7. T. Wei, A. Zifarelli, S. Dello Russo, H. Wu, G. Menduni, P. Patimisco, A. Sampaolo, V. Spagnolo, and L. Dong, "High and flat spectral responsivity of quartz tuning fork used as infrared photodetector in tunable diode laser spectroscopy," Appl. Phys. Rev. **8**(4), 041409 (2021).
8. H. Varel, D. Ashkenasi, A. Rosenfeld, M. Wähmer, and E. E. B. Campbell, "Micromachining of quartz with ultrashort laser pulses," Appl. Phys. A: Mater. Sci. Process. **65**(4-5), 367–373 (1997).
9. C. Gaudiuso, A. Volpe, and A. Ancona, "One-step femtosecond laser stealth dicing of quartz," Micromachines **11**(3), 327 (2020).
10. A. Volpe, S. Covella, C. Gaudiuso, and A. Ancona, "Improving the laser texture strategy to get superhydrophobic aluminum alloy surfaces," Coatings **11**(3), 369 (2021).
11. P. Calvani, A. Bellucci, M. Girolami, S. Orlando, V. Valentini, R. Polini, and D. M. Trucchi, "Black diamond for solar energy conversion," Carbon **105**, 401–407 (2016).
12. M. Halbwax, T. Sarnet, P. Delaporte, M. Sentis, H. Etienne, F. Torregrosa, V. Vervisch, I. Perichaud, and S. Martinuzzi, "Micro and nano-structuration of silicon by femtosecond laser: Application to silicon photovoltaic cells fabrication," Thin Solid Films **516**(20), 6791–6795 (2008).
13. N. Lasemi, U. Pacher, L. V. Zhigilei, O. Bomatí-Miguel, R. Lahoz, and W. Kautek, "Pulsed laser ablation and incubation of nickel, iron and tungsten in liquids and air," Appl. Surf. Sci. **433**, 772–779 (2018).
14. C. Gaudiuso, G. Giannuzzi, A. Volpe, P. Mario Lugarà, I. Choquet, and A. Ancona, "Incubation during laser ablation with bursts of femtosecond pulses with picosecond delays," Opt. Express **26**(4), 3801–3813 (2018).
15. S. Yan, C. Wei, H. Zou, J. Chen, Y. Li, T. Shen, A. Wang, T. Sui, and B. Lin, "Fabrication and tribological characterization of laser textured engineering ceramics: Si3N4, SiC and ZrO2," Ceram. Int. **47**(10), 13789–13805 (2021).
16. M. F. Becker, R. M. Walser, and Y. Jee, "Laser-induced damage on single-crystal metal surfaces," J. Opt. Soc. Am. B **5**(3), 648–659 (1988).
17. J. Bonse, S. Baudach, J. Krüger, W. Kautek, and M. Lenzner, "Femtosecond laser ablation of silicon-modification thresholds and morphology," Appl. Phys. A **74**(1), 19–25 (2002).
18. A. Rosenfeld, M. Lorenz, R. Stoian, and D. Ashkenasi, "Ultrashort-laser-pulse damage threshold of transparent materials and the role of incubation," Appl. Phys. A **69**, S373–S376 (1999).

19. B. Neuenschwander, B. Jaeggi, M. Schmid, A. Dommann, A. Neels, T. Bandi, and G. Hennig, "Factors controlling the incubation in the application of ps laser pulses on copper and iron surfaces," in *Laser Applications in Microelectronic and Optoelectronic Manufacturing (LAMOM) XVIII* (SPIE, 2013), 8607, p. 86070D.

20. F. Di Niso, C. Gaudiuso, T. Sibillano, F. P. Mezzapesa, A. Ancona, and P. M. Lugarà, "Influence of the Repetition Rate and Pulse Duration on the Incubation Effect in Multiple-Shots Ultrafast Laser Ablation of Steel," Phys. Procedia **41**, 698–707 (2013).

21. F. Di Niso, C. Gaudiuso, T. Sibillano, F. P. Mezzapesa, A. Ancona, and P. M. Lugarà, "Role of heat accumulation on the incubation effect in multi-shot laser ablation of stainless steel at high repetition rates," Opt. Express **22**(10), 12200 (2014).

22. J. Han, O. Malek, J. Vleugels, A. Braem, and S. Castagne, "Ultrashort pulsed laser ablation of zirconia-alumina composites for implant applications," J. Mater. Process. Technol. **299**, 117335 (2022).

23. S. Liu, Z. Li, P. B. Corkum, K. Hu, J. Yan, T. Cao, J. Peng, Z. Guo, and Q. Xu, "Energy deposition and incubation effects of nonlinear absorption of ultrashort laser pulses in dielectrics," Opt. Express **30**(7), 10317–10328 (2022).

24. G. Eberle, M. Schmidt, F. Pude, and K. Wegener, "Laser surface and subsurface modification of sapphire using femtosecond pulses," Appl. Surf. Sci. **378**, 504–512 (2016).

25. G. F. B. Almeida, L K Nolasco, G R Barbosa, A Schneider, A Jaros, I Manglano Clavero, C Margenfeld, A Waag, T Voss, and C R Mendonça, "Incubation effect during laser micromachining of GaN films with femtosecond pulses," J. Mater. Sci.: Mater. Electron. **30**(18), 16821–16826 (2019).

26. L. Qi, K. Nishii, M. Yasui, H. Aoki, and Y. Namba, "Femtosecond laser ablation of sapphire on different crystallographic facet planes by single and multiple laser pulses irradiation," Opt. Lasers Eng. **48**(10), 1000–1007 (2010).

27. J. Hernandez-Rueda, D. Puerto, J. Siegel, M. Galvan-Sosa, and J. Solis, "Plasma dynamics and structural modifications induced by femtosecond laser pulses in quartz," in *Applied Surface Science* (Elsevier B.V., 2012), 258(23), pp. 9389–9393.

28. J. M. Liu, "Simple technique for measurements of pulsed Gaussian-beam spot sizes," Opt. Lett. **7**(5), 196 (1982).

29. D. Ashkenasi, M. Lorenz, R. Stoian, and A. Rosenfeld, *Surface Damage Threshold and Structuring of Dielectrics Using Femtosecond Laser Pulses: The Role of Incubation* (n.d.), 150.

30. F. Costache, S. Eckert, and J. Reif, "Near-damage threshold femtosecond laser irradiation of dielectric surfaces: desorbed ion kinetics and defect dynamics," Appl. Phys. A **92**(4), 897–902 (2008).

31. T. Duan, Y. Li, and R. Niu, "On the mechanism of multi-pulses induced damage in dielectrics," Optik **124**(13), 1528–1531 (2013).

32. D. Gómez and I. Goenaga, "On the incubation effect on two thermoplastics when irradiated with ultrashort laser pulses: Broadening effects when machining microchannels," Appl. Surf. Sci. **253**(4), 2230–2236 (2006).

33. R. N. Oosterbeek, T. Ward, S. Ashforth, O. Bodley, A. E. Rodda, and M. C. Simpson, "Fast femtosecond laser ablation for efficient cutting of sintered alumina substrates," Opt. Lasers Eng. **84**, 105–110 (2016).

34. S. Höhm, A. Rosenfeld, J. Krüger, and J. Bonse, "Femtosecond laser-induced periodic surface structures on silica," J. Appl. Phys. **112**(1), 014901 (2012).

35. S. Xu, J. Qiu, T. Jia, C. Li, H. Sun, and Z. Xu, "Femtosecond laser ablation of crystals SiO2 and YAG," Opt. Commun. **274**(1), 163–166 (2007).

36. X. C. Wang, G. C. Lim, H. Y. Zheng, F. L. Ng, W. Liu, and S. J. Chua, "Femtosecond pulse laser ablation of sapphire in ambient air," Appl. Surf. Sci. **228**(1-4), 221–226 (2004).